



Enhanced Open-Circuit Voltage of Wide-Bandgap Perovskite Photovoltaics by Using Alloyed $(\text{FA}_{1-x}\text{Cs}_x)\text{Pb}(\text{I}_{1-x}\text{Br}_x)_3$ Quantum Dots

Mokshin Suri, Abhijit Hazarika, Bryon W. Larson, Qian Zhao, Marta Valles-Pelarda, Timothy D. Siegler, Michael K. Abney, Andrew J. Ferguson, Brian A. Korgel, and Joseph M. Luther

ACS Energy Lett., **Just Accepted Manuscript** • DOI: 10.1021/acsenerylett.9b01030 • Publication Date (Web): 16 Jul 2019

Downloaded from pubs.acs.org on July 17, 2019

Just Accepted

"Just Accepted" manuscripts have been peer-reviewed and accepted for publication. They are posted online prior to technical editing, formatting for publication and author proofing. The American Chemical Society provides "Just Accepted" as a service to the research community to expedite the dissemination of scientific material as soon as possible after acceptance. "Just Accepted" manuscripts appear in full in PDF format accompanied by an HTML abstract. "Just Accepted" manuscripts have been fully peer reviewed, but should not be considered the official version of record. They are citable by the Digital Object Identifier (DOI®). "Just Accepted" is an optional service offered to authors. Therefore, the "Just Accepted" Web site may not include all articles that will be published in the journal. After a manuscript is technically edited and formatted, it will be removed from the "Just Accepted" Web site and published as an ASAP article. Note that technical editing may introduce minor changes to the manuscript text and/or graphics which could affect content, and all legal disclaimers and ethical guidelines that apply to the journal pertain. ACS cannot be held responsible for errors or consequences arising from the use of information contained in these "Just Accepted" manuscripts.

Pursuant to the DOE Public Access Plan, this document represents the authors' peer-reviewed, accepted manuscript.
The published version of the article is available from the relevant publisher.

Enhanced Open-Circuit Voltage of Wide-Bandgap Perovskite Photovoltaics by Using Alloyed (FA_{1-x}Cs_x)Pb(I_{1-x}Br_x)₃ Quantum Dots

Mokshin Suri,^{†,‡} Abhijit Hazarika,[†] Bryon W. Larson,[†] Qian Zhao,^{†,§} Marta Vallés-Pelarda,^{||,†} Timothy D. Siegler,[‡] Michael K. Abney,[‡] Andrew J. Ferguson,[†] Brian A. Korgel,^{‡,*} and Joseph M. Luther^{†,*}

[†] National Renewable Energy Laboratory, Golden, Colorado 80401, United States

[‡] McKetta Department of Chemical Engineering and Texas Materials Institute, The University of Texas at Austin, Austin, Texas 78712-1062, United States

[§] College of Chemistry, Nankai University, Tianjin, China

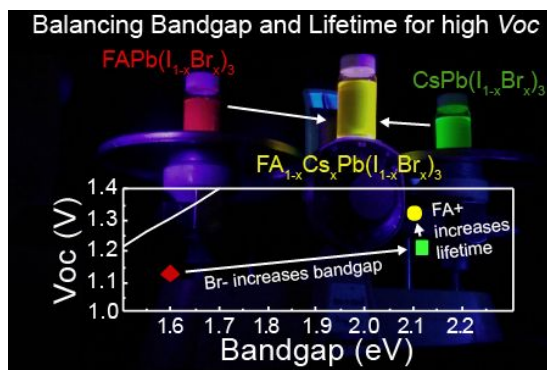
^{||} Institute of Advanced Materials (INAM), Universitat Jaume I, Avenida de Vicent Sos Baynat, s/n, 12006 Castelló de la Plana, Castellón, Spain

*Corresponding authors: joey.luther@nrel.gov; korgel@che.utexas.edu

ABSTRACT

We report a detailed study on APbX₃ (A=Formamidinium (FA⁺), Cs⁺; X=I, Br) perovskite quantum dots (PQDs) with combined A- and X-site alloying that exhibits, both, a wide bandgap and high open circuit voltage (*V*_{oc}) for the application of a potential top cell in tandem junction photovoltaic (PV) devices. The nanocrystal alloying affords control over the optical bandgap and is readily achieved by solution-phase cation and anion exchange between previously synthesized FAPbI₃ and CsPbBr₃ PQDs. Increasing only the Br⁻ content of the PQDs widens the bandgap but results in shorter carrier lifetimes and associated *V*_{oc} losses in devices. These deleterious effects can be mitigated by replacing Cs⁺ with FA⁺, resulting in wide bandgap PQD absorbers with improved charge-carrier mobility and PVs with higher *V*_{oc}. Although further device optimization is required, these results demonstrate the potential of FA_{1-x}Cs_xPb(I_{1-x}Br_x)₃ PQDs for wide bandgap perovskite PVs with high *V*_{oc}.

Table of Contents graphic:



Pursuant to the DOE Public Access Plan, this document represents the authors' peer-reviewed, accepted manuscript.
The published version of the article is available from the relevant publisher.

1
2
3 The search for high-efficiency, wide bandgap absorber materials that can be implemented
4 as a top cell in a tandem architecture to boost the overall efficiency of existing commercial
5 photovoltaic (PV) devices (e.g., Si, CIGS, CdTe) remains a challenge.¹⁻¹⁰ The tunable nature of
6 perovskite (ABX₃) absorbers, coupled with their impressive optoelectronic performance and
7 amenability to low-cost deposition techniques, identifies them as a promising candidate for such
8 applications.¹¹⁻¹⁹
9
10
11
12
13

14 Although triple-cation bulk perovskite absorbers – Cs_x(FA_yMA_(1-y))_(1-x)Pb(I_zBr_(1-z))₃ –
15 exhibit impressive solar light to electricity power conversion efficiencies (PCEs), with the current
16 PCE record at 24.2%, their bandgap (1.55-1.60 eV) is too narrow for use as the top cell in
17 multijunction PVs.^{20,21} Tuning halide composition on the X site enables wider optical bandgaps,
18 but has not led to the expected subsequent increase in *V*_{oc}, and mixed-halide bulk perovskites
19 often suffer from photoinduced halide segregation and crystal phase instability that leads to device
20 degradation.^{12,13,22-26} Perovskite quantum dots (PQDs) provide a route to circumvent these
21 structural instabilities, with the added benefit that they afford additional tunability of the optical
22 and electronic properties (by tuning the QD size and composition).^{12,13,15,22-24,27,28} For instance,
23 mixed cation PQDs with the composition FA_{1-x}Cs_xPbI₃ exhibit broader compositional tunability
24 (wider *x* range) than thin film FA_{1-x}Cs_xPbI₃. FA_{1-x}Cs_xPbI₃ PQD PVs achieve *V*_{oc}'s that approach
25 90% of the radiative limit (similar to single crystal III-V PVs, *i.e.* GaInP₂), surpassing the *V*_{oc} of
26 bulk perovskite PVs with similar composition in the bandgap range of 1.55-1.77 eV as shown in
27 Fig S1.²⁹⁻³¹ Taken together, these observations suggest that PQDs may provide an ideal solution
28 for inexpensive, high-performance, wide bandgap top cell absorber layers in multijunction PVs.
29
30
31
32
33
34
35
36
37
38
39
40

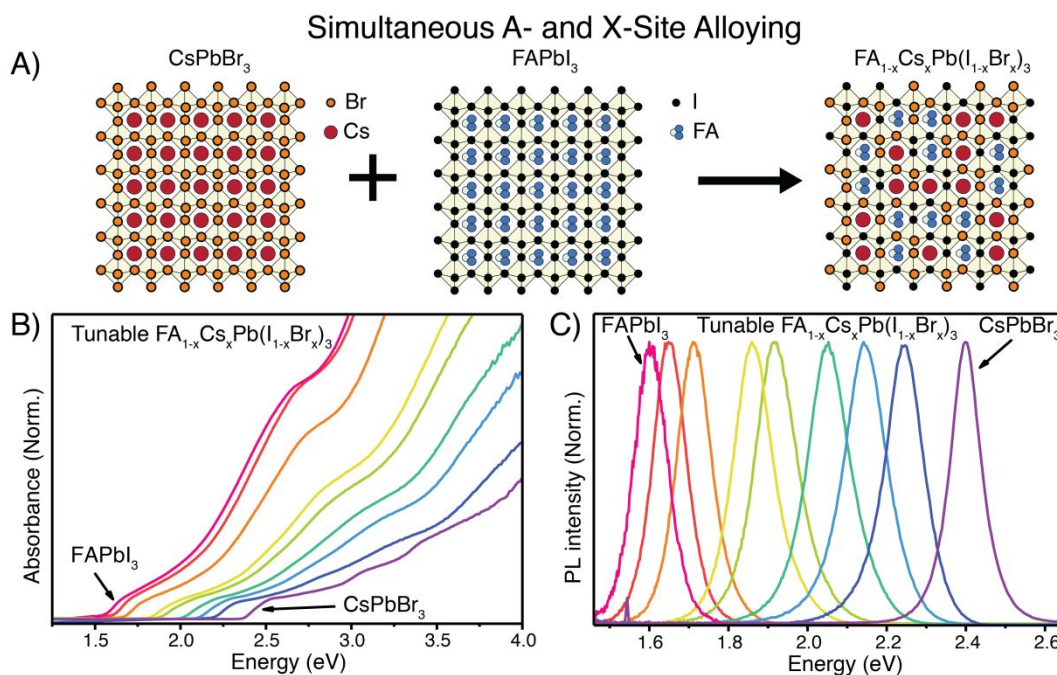
41 Wider bandgap PQDs (beyond 1.77 eV), thus far, do not show the same low *V*_{oc} losses, as
42 those with bandgap between 1.55 eV to 1.77 eV. Compositionally increasing the bandgap of PQDs
43 with Br⁻ incorporation results in a decreasing voltage fraction in PVs from 0.9 to 0.63 (in this work
44 we define voltage fraction as: device-*V*_{oc} / maximum *V*_{oc} based on device bandgap).^{22,31,32} Thus,
45 finding solutions to this unexpected voltage loss would be beneficial for the wide bandgap top cell
46 in multijunction PVs.
47
48
49
50
51

52 Here, we show that combined A- and X-site alloying of wide bandgap FA_{1-x}Cs_xPb(I_{1-x}Br_x)₃
53 PQDs can provide increased device *V*_{oc} as compared to CsPb(I_{1-x}Br_x)₃ and FAPb(I_{1-x}Br_x)₃ PQDs
54
55
56
57
58
59
60

Pursuant to the DOE Public Access Plan, this document represents the authors' peer-reviewed, accepted manuscript. The published version of the article is available from the relevant publisher.

at bandgaps wider than 1.8 eV. The addition of Br in $\text{CsPb}(\text{I}_{1-x}\text{Br}_x)_3$ PQDs—typically used to increase the bandgap—leads to a significantly decreased photoluminescence (PL) lifetime and correlates with lost V_{oc} in PVs made from these PQDs.^{22,32,33} To counter this, FA^+ was added in addition to Br to develop long PL lifetime, wide bandgap materials. This co-alloying strategy was found to improve charge transport in PQD films and reduce the voltage loss in PVs with $E_g > 1.8$ eV.

To synthesize the PQDs of such complicated composition, two simple compositions were first synthesized and alloyed using an ion exchange reaction. Fig. 1A illustrates the ion exchange between CsPbBr_3 and FAPbI_3 PQDs used to generate $\text{FA}_{1-x}\text{Cs}_x\text{Pb}(\text{I}_{1-x}\text{Br}_x)_3$ PQDs. CsPbBr_3 and FAPbI_3 PQDs were prepared using previously reported recipes.^{12,29} By mixing dispersions of FAPbI_3 and CsPbBr_3 PQDs at 70 °C, rapid and efficient compositional alloying occurs. This enables PQDs with a wide tunability of the bandgap from 1.55 eV to 2.40 eV to be obtained from similar starting materials simply by controlling the relative amount of CsPbBr_3 to FAPbI_3 in the ion-exchange reaction. Figs. 1B and 1C show absorbance and PL spectra of PQDs generated from the same CsPbBr_3 and FAPbI_3 PQDs starting materials. The nanocrystals retain a relatively narrow size distribution comparable to the starting materials.



Pursuant to the DOE Public Access Plan, this document represents the authors' peer-reviewed, accepted manuscript.
The published version of the article is available from the relevant publisher.

Figure 1. A) Crystal models showing the ion exchange process used to generate alloyed PQDs. $FA_{1-x}Cs_xPb(I_{1-x}Br_x)_3$ PQDs are generated when dispersions of $CsPbBr_3$ and $FAPbI_3$ PQDs are mixed at 70°C. Room temperature **(B)** absorbance and **(C)** PL emission spectra of PQDs with varying $FA_{1-x}Cs_xPb(I_{1-x}Br_x)_3$ composition dispersed in octane (excitation wavelength of 400 nm).

We first highlight the deleterious effects of Br⁻ incorporation in single A-site PQD PVs by using colloidal PQDs with bandgaps ranging between 1.8 eV and 1.94 eV containing only Cs⁺ on the A-site. Unlike PQDs of $FA_{1-x}Cs_xPb(I_{1-x}Br_x)_3$ composition, $CsPb(I_{1-x}Br_x)_3$ and $FAPb(I_{1-x}Br_x)_3$ PQDs were synthesized using previously reported methods of single-pot direct synthesis using controlled ratios of Pb-halide salts.¹² Fig. 2A shows a scanning electron microscopy (SEM) image of a cross-sectioned $CsPbI_3$ PQD PV. The PQD solar cells were fabricated using previously reported methods.^{34–37} For ideal removal of the oleate ligands, it is especially important to maintain an ambient environment that exhibits 15–25% relative humidity (RH) during the ligand exchange procedure performed after deposition of the nanocrystals.³⁵ Fig. 2B shows the device responses of $CsPbI_3$ PQDs and $CsPb(I_{1-x}Br_x)_3$ PQD PVs with Br⁻ alloying to widen the bandgap. The $CsPbI_3$ PQD PV exhibits a PCE of ~14% (reverse scan). The $CsPb(I_{1-x}Br_x)_3$ PQD PVs have lower device efficiency, which can be expected based on the widened bandgap and corresponding reduced light absorption; however, they also show a decrease in the V_{oc} contrary to the expectations for the widened bandgap with increased Br⁻ content. A noticeable drop in fill factor is also observed with increasing Br⁻ incorporation, which suggests increased series resistance in the device possibly originating from non-ideal contact layers in the device structure. Full device metrics for the devices shown in Figure 2B are provided in Table S1 as Supporting Information.

Pursuant to the DOE Public Access Plan, this document represents the authors' peer-reviewed, accepted manuscript. The published version of the article is available from the relevant publisher.

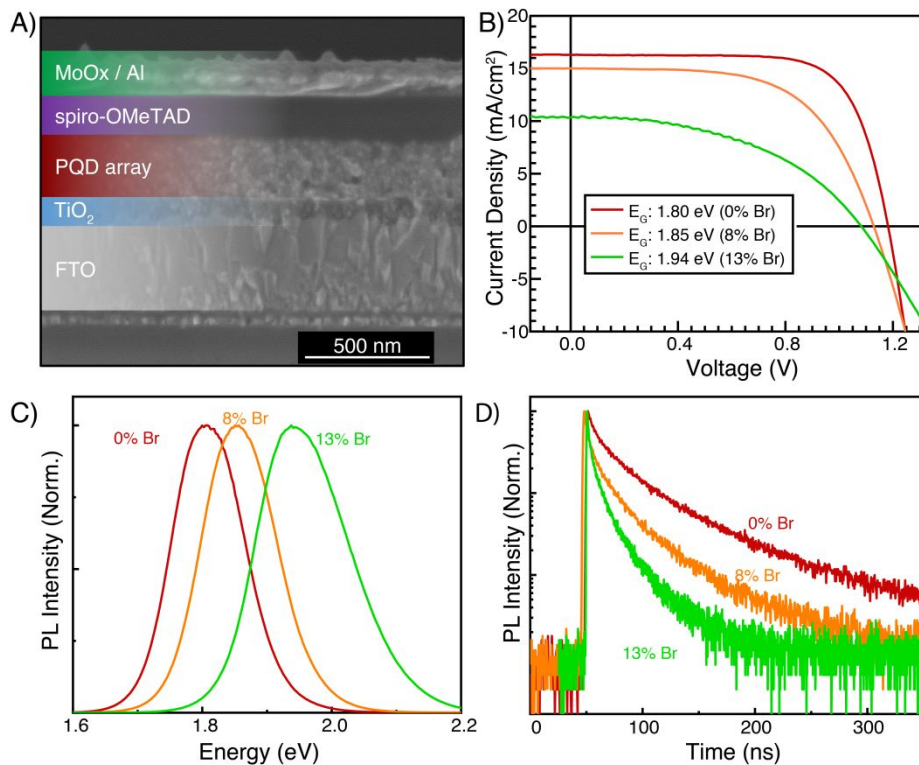


Figure 2. **A)** SEM image of a cross-sectioned CsPbI₃ PVD PV device. **B)** J/V curves of CsPb(I_xBr_{1-x})₃ PVDs with varying Br composition and bandgap. Note that the reported bandgaps correspond to the PL peak energies. The device absorption onset is redshifted by 0.05-0.1 eV due to electronic coupling.^{17,33} **C)** Room temperature normalized PL emission spectra of the colloidal PVDs used to fabricate devices tested in (B). Excitation wavelength was 400 nm. **D)** Time-resolved PL transients of the CsPb(I_xBr_{1-x})₃ PVDs used to make the devices from panel B. The excitation wavelength is 442 nm and the emission are collected at the PL peak position.

Figs. 2C and 2D show solution-phase photoluminescence (PL) emission spectra and solution-phase time-resolved photoluminescence (TRPL) measurements on CsPbI₃ PVDs compared to CsPb(I_{1-x}Br_x)₃ PVDs with 8% and 13% Br compositions. The composition of all PVD samples in this work are estimated using Vegard's Law.³⁸ As expected, the increase in the Br/I ratio results in a hypsochromic shift of the PL spectrum, but the mixed anion systems also exhibit broadening of the emission spectrum, which may be related to an increase in the polydispersity of the PVDs or a non-uniform anion composition within the ensemble. We find that CsPb(I_{1-x}Br_x)₃ PVDs show significantly reduced PL lifetime compared to the CsPbI₃ PVDs. Based on previous reports, we believe that increased Br composition leads to higher PL quantum yield and decreased PL lifetime, which suggests that shorter radiative lifetimes are intrinsic to Br-rich

Pursuant to the DOE Public Access Plan, this document represents the authors' peer-reviewed, accepted manuscript.
The published version of the article is available from the relevant publisher.

1
2
3 PQDs.^{11,13,15,17} See Supporting Information Figure S2 for a plot summarizing the radiative lifetimes
4 versus bandgap and Br⁻ content of PQDs samples. From the results in Fig. 2, we hypothesize that
5 increased bromine content in PQDs leads to a decreased PL lifetime, and that the PL lifetime of
6 colloidal PQDs is related to PQD device performance, especially the deteriorating *V_{oc}*
7 performance at wide bandgaps as discussed above.
8
9

10
11 To test this hypothesis, TRPL measurements of several colloidal PQD compositions
12 (CsPb(I_{1-x}Br_x)₃, FAPb(I_{1-x}Br_x)₃, and FA_{1-x}Cs_xPb(I_{1-x}Br_x)₃) were conducted using a streak-camera
13 system that records spectral- and time-dependent emission data. Fig. 3A shows two-dimensional
14 solution-phase TRPL data for CsPbI₃ colloidal PQDs, and the red-dashed box in Fig. 3A shows
15 the region of the response that is integrated to produce a TRPL transient decay curve. The inset in
16 Fig. 3A shows the actual transient that is extracted from the streak camera response. While the
17 TRPL measurements were performed in the solution phase, we believe that the reduced PL lifetime
18 of colloidal CsPb(I_{1-x}Br_x)₃ PQDs is at least partly related to the observed loss in device *V_{oc}*. To
19 overcome this, we aimed to lengthen the PL lifetime of these PQDs through compositional
20 alloying. While that challenge at face value is not so straightforward, it has been reported that
21 FAPbI₃ QDs have substantially longer PL lifetime than CsPbI₃, but unfortunately replacing Cs⁺
22 with FA⁺ also lowers the bandgap.³⁹ We, therefore, hypothesized that by balancing the FA⁺ to Cs⁺,
23 along with the Br⁻ to I⁻, we could engineer the PQDs to have an appropriate bandgap (from Br⁺
24 incorporation) with lengthened PL lifetimes (from FA⁺ incorporation). To test this specific
25 hypothesis, we show in Fig. 3B, CsPb(I_{1-x}Br_x)₃, FAPb(I_{1-x}Br_x)₃, and FA_{1-x}Cs_xPb(I_{1-x}Br_x)₃ colloidal
26 PQDs each with composition tuned to achieve a bandgap of approximately 1.9 eV. The TRPL
27 transients show that FA⁺ incorporation nearly doubles the lifetime from 29 ns to 55 ns for the
28 FA⁺/Cs⁺ alloy-sample or 64 ns for the sample with pure FA⁺ on the A-site. Thus, in this case, the
29 A-site mediated lengthening of the PL lifetime overrules X-site mediated PL lifetime shortening.
30
31
32
33
34
35
36
37
38
39
40
41
42
43
44
45
46
47
48
49
50
51
52
53
54
55
56
57
58
59
60

Pursuant to the DOE Public Access Plan, this document represents the authors' peer-reviewed, accepted manuscript. The published version of the article is available from the relevant publisher.

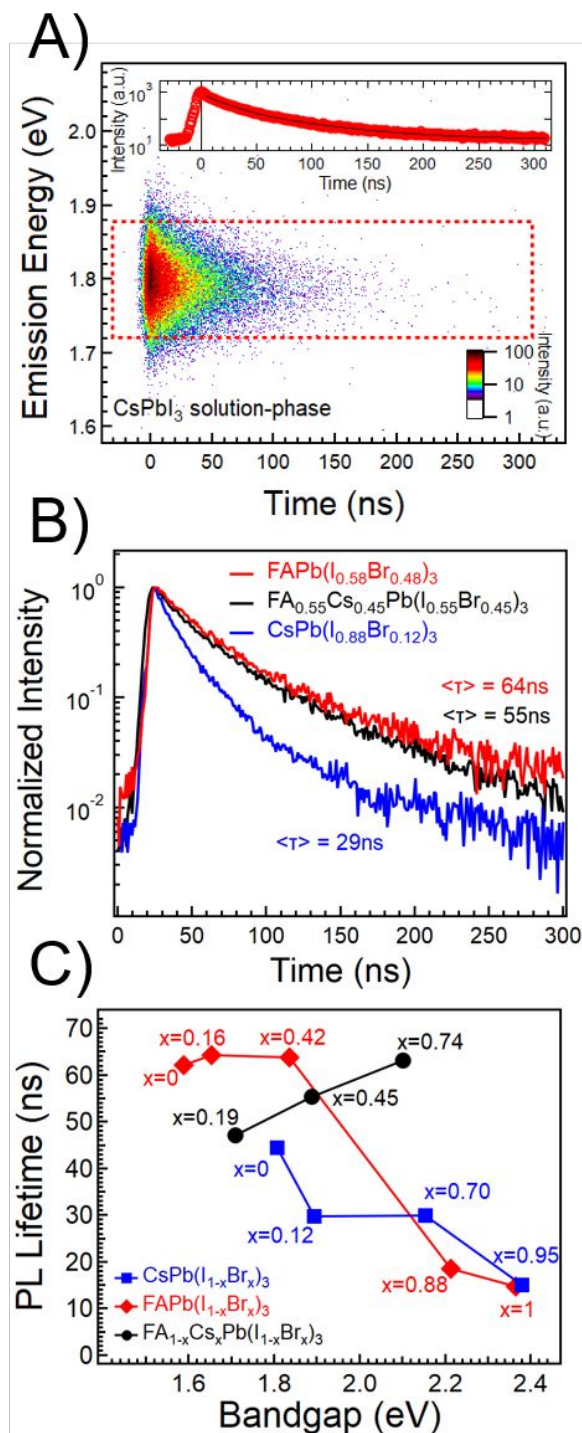


Figure 3. **A)** Two-dimensional spectrotemporal solution-phase TRPL data of CsPbI₃ PQDs, measured using a streak-camera. The red rectangle represents the portion of the trace that was integrated to construct an intensity versus decay-time transient. **B)** Solution-phase TRPL transients of CsPb(I_{1-x}Br_x)₃, FAPb(I_{1-x}Br_x)₃ and FA_{1-x}Cs_xPb(I_{1-x}Br_x)₃ solution-phase PQDs with bandgap energies of ca. 1.9 eV. (These PQD

Pursuant to the DOE Public Access Plan, this document represents the authors' peer-reviewed, accepted manuscript.
The published version of the article is available from the relevant publisher.

1
2
3 compositions are estimated using Vegard's Law based on the PL peak energy.³⁸ C) Intensity-averaged
4 PL lifetime versus bandgap of all solution-phase PQD samples including CsPb(I_{1-x}Br_x)₃, FAPb(I_{1-x}Br_x)₃,
5 and FA_{1-x}Cs_xPb(I_{1-x}Br_x)₃ PQDs. See Fig. S2 for the estimated radiative lifetime-component versus
6 bandgap of each sample.
7
8
9

10
11 As shown in Figs. 2D and 3B, the solution-phase intensity-averaged TRPL decays cannot
12 be described by a single-exponential function. While the origin of this deviation from simple first-
13 order decay kinetics is beyond the scope of this work, we analyze our data with a bi-exponential
14 decay and compare the intensity-weighted average PL lifetimes (Fig. 3C) of the CsPb(I_{1-x}Br_x)₃,
15 FAPb(I_{1-x}Br_x)₃, and FA_{1-x}Cs_xPb(I_{1-x}Br_x)₃ PQDs as a function of bandgap. The intensity-weighted
16 average PL lifetime of the CsPb(I_{1-x}Br_x)₃ PQDs decreases significantly from about 45 ns to 15 ns
17 across the compositional range, with a sharp decrease observed even for small bromide contents
18 (c.f. Fig. 2D). In contrast, the FAPb(I_{1-x}Br_x)₃ and FA_{1-x}Cs_xPb(I_{1-x}Br_x)₃ PQDs appear to be less
19 sensitive to the substitution of I⁻ with Br⁻. Single-cation FAPb(I_{1-x}Br_x)₃ PQDs exhibit similar
20 lifetimes of >60 ns until the bandgap exceeds 1.8 eV (Br⁻ content of 42%) where the lifetime drops
21 precipitously to 15 ns, similar to the average lifetimes observed for the single-cation Cs-containing
22 PQDs. The mixed-cation FA_{1-x}Cs_xPb(I_{1-x}Br_x)₃ PQDs, on the other hand, exhibit PL lifetimes that
23 actually increase with bandgap energy, and reach 65 ns for a bandgap of 2.1 eV. To our
24 knowledge, this increase in PL lifetime with increasing bandgap for the FA_{1-x}Cs_xPb(I_{1-x}Br_x)₃
25 composition is unique among PQDs. The full set of TRPL decay transient data and fitting
26 parameters are provided as Supporting Information in Fig. S3 and Table S2.
27
28
29
30
31
32
33
34
35
36
37
38

39 To explore the impact of the observed colloidal-optoelectronic properties of the PQDs on
40 their PV performance, solar cells were fabricated with CsPb(I_{1-x}Br_x)₃, FAPb(I_{1-x}Br_x)₃, and FA<sub>1-
41 x</sub>Cs_xPb(I_{1-x}Br_x)₃ PQDs with bandgaps ranging from 1.55 eV to 2.15 eV. Fig. 4A plots the *V*_{oc} of
42 over 140 PQD PVs with 10 different compositions across a wide alloy-space and bandgap regime.
43 By displaying results from a large sample set, we are able to determine which composition of
44 PQDs provides the most promise for use as wide-bandgap top cells in tandem devices. Of the PQD
45 devices, those with A-site alloying of FA⁺ and Cs⁺ exhibit the highest *V*_{oc} at bandgaps wider than
46 1.8 eV. This trend is especially noticeable at bandgap of ~1.85 eV where the *V*_{oc} increases by
47 over 100 mV as the PQD composition is changed from CsPb(I_{0.88}Br_{0.12})₃ to FAPb(I_{0.58}Br_{0.42})₃ to
48
49
50
51
52
53
54
55
56
57
58
59
60

Pursuant to the DOE Public Access Plan, this document represents the authors' peer-reviewed, accepted manuscript.
The published version of the article is available from the relevant publisher.

1
2
3 FA_{0.45}Cs_{0.55}Pb(I_{0.55}Br_{0.45})₃. At a bandgap of ~2.1 eV, the maximum V_{oc} of the FA_{1-x}Cs_xPb(I_{1-x}Br_x)₃
4 PQD devices was about 100 mV higher than that of CsPb(I_{1-x}Br_x)₃ PQD PVs. Fig. 4B shows a
5 plot of the voltage fraction against the bandgap of the PQD PVs. Voltage fraction decreases with
6 increasing Br⁻ incorporation and widening bandgap. The PVs of FAPbI₃ PQDs with a bandgap of
7 1.55 eV exhibit the highest voltage fraction of ~0.9 and the PL lifetime of these PQDs is 62 ns.
8 (Note: in Fig. S1 we plot the voltage fraction of our PQD PVs against perovskite-literature values
9 to compare our results to the immense field of perovskite PV and show the future promise of PQD
10 PVs).
11
12
13
14
15
16
17
18
19
20
21
22
23
24
25
26
27
28
29
30
31
32
33
34
35
36
37
38
39
40
41
42
43
44
45
46
47
48
49
50
51
52
53
54
55
56
57
58
59
60

Pursuant to the DOE Public Access Plan, this document represents the authors' peer-reviewed, accepted manuscript. The published version of the article is available from the relevant publisher.

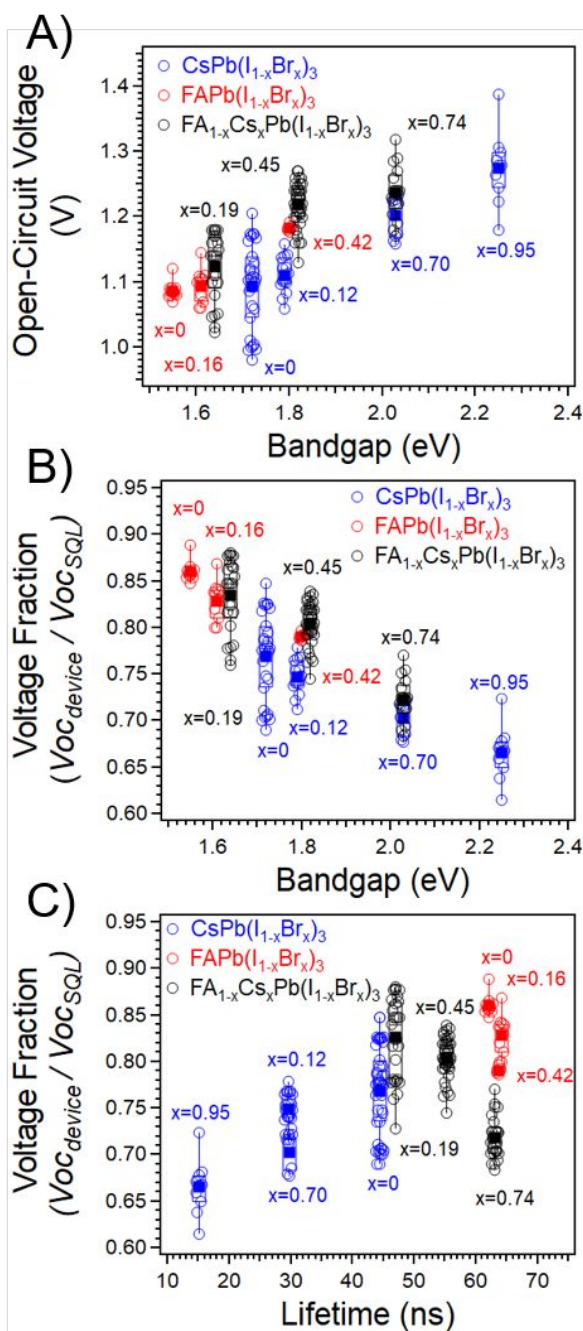


Figure 4 A) V_{oc} versus bandgap of the full set of PQD samples B) Voltage fraction versus bandgap of the full data set of PQD samples. C) Voltage fraction versus PL lifetime of the full data set of PQD samples. Full device metrics are provided as Supporting Information (Table S3).

Pursuant to the DOE Public Access Plan, this document represents the authors' peer-reviewed, accepted manuscript.
The published version of the article is available from the relevant publisher.

To test our hypothesis that PQD PV voltage performance is correlated to PL lifetime of colloidal PQDs, we plot voltage fraction of PQD PVs versus PL lifetime of solution-phase PQDs in Fig. 4C. We observe that $\text{CsPb}(\text{I}_{1-x}\text{Br}_x)_3$ PQDs show a fairly direct relationship between solution-phase PL lifetime and device voltage fraction. However, the voltage fraction of $\text{FAPb}(\text{I}_{1-x}\text{Br}_x)_3$ PQDs demonstrates a more compositional dependence - the voltage fraction of $\text{FAPb}(\text{I}_{1-x}\text{Br}_x)_3$ PQDs increases as the Br composition decreases. The fully alloyed PQDs ($\text{FA}_{1-x}\text{Cs}_x\text{Pb}(\text{I}_{1-x}\text{Br}_x)_3$) generally exhibit voltage fraction between 0.70 and 0.85, which is comparable to current, state-of-the-art bulk-phase CsPbI_3 devices (See Fig S1).⁴⁰ Although the A- and X-site alloying of $\text{FA}_{1-x}\text{Cs}_x\text{Pb}(\text{I}_{1-x}\text{Br}_x)_3$ PQDs succeeded in producing devices with higher V_{oc} at wide bandgaps, the PCE was still low—only 6% for a bandgap of 1.9 eV. We attribute these observations of lower PCE and the slight drop in voltage fraction of $\text{FA}_{1-x}\text{Cs}_x\text{Pb}(\text{I}_{1-x}\text{Br}_x)_3$ PQDs, as “x” increases from 0.45-0.74, to poor charge transport in the PQD films and/or carrier extraction at the contact layers, which limits the J_{sc} and FF of the devices (see Supporting Information Table S3). We employed time-resolved microwave conductivity (TRMC) to determine how the A-site and X-site alloying influences the charge transport in the PQD films. The photoconductance, ΔG , extracted from the TRMC data can be related to a free-carrier yield-mobility product, $\phi\Sigma\mu$, which can be difficult to decompose into the individual contributions.^{41,42} However, the large dielectric constant of PQDs and large photoluminescence lifetimes (>20 ns) allows us to make the assumption that each photon generates an unbound electron-hole pair on the 4 ns timescale of the laser pulse in the TRMC measurement (i.e., $\phi = 1$), which simplifies the figure of merit to sum of carrier mobilities.⁴² Although we are able to make assumptions about the free-carrier yield, we cannot decouple the individual contributions of the electrons and holes to the photoconductance. Under such circumstances, the TRMC technique can be considered similar to other optical pump-probe techniques, except that the sum of the free-carrier mobilities, $\Sigma\mu$, now represents the absorption coefficient of the microwave probe. The transient photoconductance, $\Delta G(t)$, is therefore related to the number density, and associated kinetics, of the free electrons and holes in the PQD layer. Since we expect both carriers to contribute to the measured photoconductance, and the carrier lifetime to be related to the likelihood of the carriers to be extracted in a functioning device, we suggest that the yield-mobility-tau product represents a reasonable metric to describe the free-carrier transport and dynamics (in fact, this quantity can be related to the carrier diffusion length).

Pursuant to the DOE Public Access Plan, this document represents the authors' peer-reviewed, accepted manuscript. The published version of the article is available from the relevant publisher.

Fig. 5 shows the yield-mobility-tau products determined by TRMC of the ligand-exchanged PQD films on quartz substrates (the TRMC yield-mobilities and free carrier lifetimes are also provided as Supporting Information Fig.S4-S5). In all cases, the yield is assumed to be 1, meaning that we expect all charge carriers to diffuse, the mobility describes the sum of hole and electron mobility, and carrier lifetime takes into consideration all holes and electrons. CsPbI₃ PQDs show the largest yield-mobility-tau product at $\sim 500 * 10^{-9} \text{ cm}^2/\text{V}$. The yield-mobility-tau product decreases logarithmically with increasing bandgap for single A-site PQDs, indicating that charge transport becomes less efficient with increasing Br composition. For FA_{1-x}Cs_xPb(I_{1-x}Br_x)₃ PQDs, the yield-mobility-tau product remains fairly stable across all three samples ($\sim 30\text{-}50 * 10^{-9} \text{ cm}^2/\text{V}$), and the 2.1 eV bandgap FA_{1-x}Cs_xPb(I_{1-x}Br_x)₃ PQDs leads to an enhanced yield-mobility-tau product over the single A-site PQDs with similar bandgap. Thus, at wide bandgaps, simultaneous alloying at the A- and X-sites leads to increased charge transport, but there is still room for improvement because the yield-mobility-tau products of FA_{1-x}Cs_xPb(I_{1-x}Br_x)₃ PQDs are an order of magnitude less than that of CsPbI₃. Improvements in PQD synthesis, purification, and device fabrication are potential methods to improve charge transport in these films and improve PCE.

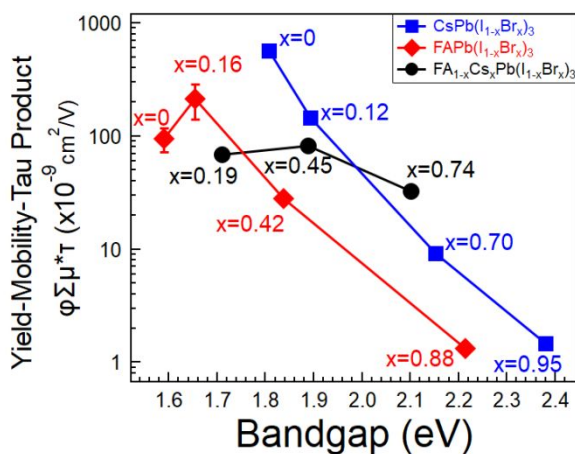


Figure 5. Yield-mobility-tau product determined by TRMC of CsPb(I_{1-x}Br_x)₃, FAPb(I_{1-x}Br_x)₃, and FA_{1-x}Cs_xPb(I_{1-x}Br_x)₃ PQD films on quartz substrates.

In conclusion, we show that the substitution of I for Br in metal halide PQDs results in faster electron-hole recombination, less efficient charge transport, and significant loss in device

Pursuant to the DOE Public Access Plan, this document represents the authors' peer-reviewed, accepted manuscript. The published version of the article is available from the relevant publisher.

V_{oc}, that hinders their performance in PQD PV devices. Simultaneous alloying on the A-site with Cs⁺ and FA⁺ to generate FA_{1-x}Cs_xPb(I_{1-x}Br_x)₃ PQDs counteracts these adverse effects of increased Br content. To our knowledge, FA_{1-x}Cs_xPb(I_{1-x}Br_x)₃ PQDs are the only PQDs to exhibit longer PL lifetimes with increased bandgap. The *V_{oc}* of FA_{1-x}Cs_xPb(I_{1-x}Br_x)₃ PQDs with bandgaps larger than 1.8 eV exhibit *V_{oc}* nearly 100 mV higher than CsPb(I_{1-x}Br_x)₃ PQDs of similar bandgap. While further optimization of wide bandgap PQD PVs is needed, these results suggest considerable promise for the continued improvement of wide bandgap perovskite PV device layers needed for high-efficiency, low-cost multijunction solar cells.

Supporting Information. Experimental methods, characterizations, absorbance and photoluminescence of colloidal PQDs, TRPL transients including fitting parameters of colloidal PQDs, estimated radiative lifetimes for all colloidal PQD compositions, device metrics for PQD PVs in Fig. 2, device metrics for all other PQD PVs for this study, TRMC lifetime of PQD thin films, and TRMC yield-mobility product of PQD thin films.

Author Information

Corresponding Authors

Email: joey.luther@nrel.gov

Email: korgel@che.utexas.edu

Notes

The authors declare no competing financial interest.

Acknowledgements. This work was authored in part by the National Renewable Energy Laboratory, operated by Alliance for Sustainable Energy, LLC, for the U.S. Department of Energy (DOE) under Contract No. DE-AC36-08GO28308. The QD synthesis was developed in the Laboratory Directed Research and Development program at NREL. The QD device fabrication acknowledges the Operational Energy Capability Improvement Fund of the Department of Defense. Time-resolved characterization at NREL was funded by the U.S. Department of Energy Office of Energy Efficiency and Renewable Energy Solar Energy Technologies Office. Funding

Pursuant to the DOE Public Access Plan, this document represents the authors' peer-reviewed, accepted manuscript.
The published version of the article is available from the relevant publisher.

1
2
3 for the work at The University of Texas was provided by the Robert A. Welch Foundation (F-
4 1464) and the National Science Foundation through the Industry/University Cooperative Research
5 Center (IUCRC) for Next Generation Photovoltaics (IIP-1540028 and IIP-1822206). M.S. would
6 like to acknowledge the U.S. DOE, Office of Science, Office of Workforce Development for
7 Teachers and Scientists, Science Undergraduate Laboratory Internship (SULI) Program for
8 funding in 2017 and 2018. Q.Z. acknowledges fellowship support from the China Scholarship
9 Council and Natural Science of Foundation China (21576140). M.V.-P. acknowledges Universitat
10 Jaume I (UJI) through FPI Fellowship Program (PREDOC/2017/40) and (E-2018-14) within
11 framework of Action 2 of the Mobility Program for Research Staff under the 2018 Research
12 Promotion Plan. TDS acknowledges United States government support under and awarded by
13 DoD, Air Force Office of Scientific Research, National Defense Science and Engineering
14 Graduate (NDSEG) Fellowship, 32 CFR 168a. The views expressed in the article do not
15 necessarily represent the views of the DOE or the U.S. Government.
16
17
18
19
20
21
22
23
24
25
26
27
28

29 References

- 30
31
32
33 (1) McMeekin, D. P.; Sadoughi, G.; Rehman, W.; Eperon, G. E.; Saliba, M.; Hörantner,
34 M. T.; Haghighirad, A.; Sakai, N.; Korte, L.; Rech, B.; et al. A Mixed-Cation Lead
35 Mixed-Halide Perovskite Absorber for Tandem Solar Cells. *Science* **2016**, *351*,
36 151–155.
37
38
39 (2) Vos, A. D. Detailed Balance Limit of the Efficiency of Tandem Solar Cells. *J. Phys.*
40 *D Appl. Phys.* **1980**, *13*, 839–846.
41
42 (3) Karani, A.; Yang, L.; Bai, S.; Futscher, M. H.; Snaith, H. J.; Ehrler, B.; Greenham,
43 N. C.; Di, D. Perovskite/Colloidal Quantum Dot Tandem Solar Cells: Theoretical
44 Modeling and Monolithic Structure. *ACS Energy Lett.* **2018**, *3*, 869–874.
45
46 (4) Correa-Baena, J.-P.; Saliba, M.; Buonassisi, T.; Grätzel, M.; Abate, A.; Tress, W.;
47 Hagfeldt, A. Promises and Challenges of Perovskite Solar Cells. *Science* **2017**,
48 *358*, 739–744.
49
50
51
52
53
54
55
56
57
58
59
60

Pursuant to the DOE Public Access Plan, this document represents the authors' peer-reviewed, accepted manuscript.
The published version of the article is available from the relevant publisher.

- (5) Zhao, D.; Yu, Y.; Wang, C.; Liao, W.; Shrestha, N.; Grice, C. R.; Cimaroli, A. J.; Guan, L.; Ellingson, R. J.; Zhu, K.; et al. Low-Bandgap Mixed Tin–Lead Iodide Perovskite Absorbers with Long Carrier Lifetimes for All-Perovskite Tandem Solar Cells. *Nat. Energy* **2017**, *2*, 17018
- (6) Eperon, G. E.; Leijtens, T.; Bush, K. A.; Prasanna, R.; Green, T.; Wang, J. T.-W.; McMeekin, D. P.; Volonakis, G.; Milot, R. L.; May, R.; et al. Perovskite-Perovskite Tandem Photovoltaics with Optimized Band Gaps. *Science* **2016**, *354*, 861–865.
- (7) Han, Q.; Hsieh, Y.-T.; Meng, L.; Wu, J.-L.; Sun, P.; Yao, E.-P.; Chang, S.-Y.; Bae, S.-H.; Kato, T.; Bermudez, V.; et al. High-Performance Perovskite/Cu(In,Ga)Se₂ Monolithic Tandem Solar Cells. *Science* **2018**, *361*, 904–908.
- (8) Bush, K. A.; Palmstrom, A. F.; Yu, Z. J.; Boccard, M.; Cheacharoen, R.; Mailoa, J. P.; McMeekin, D. P.; Hoyer, R. L. Z.; Bailie, C. D.; Leijtens, T.; et al. 23.6%-Efficient Monolithic Perovskite/Silicon Tandem Solar Cells with Improved Stability. *Nat. Energy* **2017**, *2*, 17009.
- (9) Beal, R. E.; Slotcavage, D. J.; Leijtens, T.; Bowring, A. R.; Belisle, R. A.; Nguyen, W. H.; Burkhard, G. F.; Hoke, E. T.; McGehee, M. D. Cesium Lead Halide Perovskites with Improved Stability for Tandem Solar Cells. *J. Phys. Chem. Lett.* **2016**, *7*, 746–751.
- (10) Siegler, T. D.; Shimpi, T. M.; Sampath, W. S.; Korgel, B. A. Development of Wide Bandgap Perovskites for Next-Generation Low-Cost CdTe Tandem Solar Cells. *Chemical Engineering Science* **2019**, *199*, 388–397.
- (11) Becker, M. A.; Vaxenburg, R.; Nedelcu, G.; Sercel, P. C.; Shabaev, A.; Mehl, M. J.; Michopoulos, J. G.; Lambrakos, S. G.; Bernstein, N.; Lyons, J. L.; et al. Bright Triplet Excitons in Caesium Lead Halide Perovskites. *Nature* **2018**, *553*, 189–193.
- (12) Protesescu, L.; Yakunin, S.; Bodnarchuk, M. I.; Krieg, F.; Caputo, R.; Hendon, C. H.; Yang, R. X.; Walsh, A.; Kovalenko, M. V. Nanocrystals of Cesium Lead Halide Perovskites (CsPbX₃, X = Cl, Br, and I): Novel Optoelectronic Materials Showing Bright Emission with Wide Color Gamut. *Nano Lett.* **2015**, *15*, 3692–3696.
- (13) Akkerman, Q. A.; D’Innocenzo, V.; Accornero, S.; Scarpellini, A.; Petrozza, A.; Prato, M.; Manna, L. Tuning the Optical Properties of Cesium Lead Halide

Pursuant to the DOE Public Access Plan, this document represents the authors' peer-reviewed, accepted manuscript.
The published version of the article is available from the relevant publisher.

- 1
2
3
4 Perovskite Nanocrystals by Anion Exchange Reactions. *J. Am. Chem. Soc.* **2015**,
5 *137*, 10276–10281.
6
7 (14) Pan, J.; Shang, Y.; Yin, J.; De Bastiani, M.; Peng, W.; Dursun, I.; Sinatra, L.; El-
8 Zohry, A. M.; Hedhili, M. N.; Emwas, A.-H.; et al. Bidentate Ligand-Passivated
9 CsPbI₃ Perovskite Nanocrystals for Stable Near-Unity Photoluminescence
10 Quantum Yield and Efficient Red Light-Emitting Diodes. *J. Am. Chem. Soc.* **2018**,
11 *140*, 562–565.
12
13 (15) Nedelcu, G.; Protesescu, L.; Yakunin, S.; Bodnarchuk, M. I.; Grotevent, M. J.;
14 Kovalenko, M. V. Fast Anion-Exchange in Highly Luminescent Nanocrystals of
15 Cesium Lead Halide Perovskites (CsPbX₃, X = Cl, Br, I). *Nano Lett.* **2015**, *15*, 5635–
16 5640.
17
18 (16) Wu, L.; Zhong, Q.; Yang, D.; Chen, M.; Hu, H.; Pan, Q.; Liu, H.; Cao, M.; Xu, Y.;
19 Sun, B.; et al. Improving the Stability and Size Tunability of Cesium Lead Halide
20 Perovskite Nanocrystals Using Trioctylphosphine Oxide as the Capping Ligand.
21 *Langmuir* **2017**, *33*, 12689–12696.
22
23 (17) Swarnkar, A.; Marshall, A. R.; Sanehira, E. M.; Chernomordik, B. D.; Moore, D. T.;
24 Christians, J. A.; Chakrabarti, T.; Luther, J. M. Quantum Dot-Induced Phase
25 Stabilization of α -CsPbI₃ Perovskite for High-Efficiency Photovoltaics. *Science*
26 **2016**, *354*, 92–95.
27
28 (18) Chen, Q.; Wu, J.; Ou, X.; Huang, B.; Almutlaq, J.; Zhumekenov, A. A.; Guan, X.;
29 Han, S.; Liang, L.; Yi, Z.; et al. All-Inorganic Perovskite Nanocrystal Scintillators.
30 *Nature* **2018**, *561*, 88–93.
31
32 (19) Talapin, D. V.; Lee, J.-S.; Kovalenko, M. V.; Shevchenko, E. V. Prospects of
33 Colloidal Nanocrystals for Electronic and Optoelectronic Applications. *Chemical*
34 *Reviews* **2010**, *110*, 389–458.
35
36 (20) Saliba, M.; Matsui, T.; Seo, J.-Y.; Domanski, K.; Correa-Baena, J.-P.; Nazeeruddin,
37 M. K.; Zakeeruddin, S. M.; Tress, W.; Abate, A.; Hagfeldt, A.; et al. Cesium-
38 Containing Triple Cation Perovskite Solar Cells: Improved Stability, Reproducibility
39 and High Efficiency. *Energy & Environmental Science* **2016**, *9*, 1989–1997.
40
41
42
43
44
45
46
47
48
49
50
51
52
53
54
55
56
57
58
59
60

Pursuant to the DOE Public Access Plan, this document represents the authors' peer-reviewed, accepted manuscript.
The published version of the article is available from the relevant publisher.

- 1
2
3
4 (21) NREL. Best Research-Cell Efficiencies. [https://www.nrel.gov/pv/cell-](https://www.nrel.gov/pv/cell-efficiency.html)
5 [efficiency.html](https://www.nrel.gov/pv/cell-efficiency.html). (accessed June 17, 2019).
6
7 (22) Christodoulou, S.; Di Stasio, F.; Pradhan, S.; Stavrinadis, A.; Konstantatos, G.
8 High-Open-Circuit-Voltage Solar Cells Based on Bright Mixed-Halide CsPbBr₂
9 Perovskite Nanocrystals Synthesized under Ambient Air Conditions. *J. Phys.*
10 *Chem. C* **2018**, *122*, 7621–7626.
11
12 (23) Gualdrón-Reyes, A. F.; Yoon, S. J.; Barea, E. M.; Agouram, S.; Muñoz-Sanjosé, V.;
13 Meléndez, Á. M.; Niño-Gómez, M. E.; Mora-Seró, I. Controlling the Phase
14 Segregation in Mixed Halide Perovskites through Nanocrystal Size. *ACS Energy*
15 *Lett.* **2019**, *4*, 54–62.
16
17 (24) Wang, X.; Ling, Y.; Lian, X.; Xin, Y.; Dhungana, K. B.; Perez-Orive, F.; Knox, J.;
18 Chen, Z.; Zhou, Y.; Beery, D.; et al. Suppressed Phase Separation of Mixed-Halide
19 Perovskites Confined in Endotaxial Matrices. *Nat. Commun.* **2019**, *10*, 695.
20
21 (25) Slotcavage, D. J.; Karunadasa, H. I.; McGehee, M. D. Light-Induced Phase
22 Segregation in Halide-Perovskite Absorbers. *ACS Energy Lett.* **2016**, *1*, 1199–
23 1205.
24
25 (26) Zeng, Q.; Zhang, X.; Feng, X.; Lu, S.; Chen, Z.; Yong, X.; Redfern, S. A. T.; Wei,
26 H.; Wang, H.; Shen, H.; et al. Polymer-Passivated Inorganic Cesium Lead Mixed-
27 Halide Perovskites for Stable and Efficient Solar Cells with High Open-Circuit
28 Voltage over 1.3 V. *Adv. Mater.* **2018**, *30*, 1705393.
29
30 (27) Hoffman, J. B.; Zaiats, G.; Wappes, I.; Kamat, P. V. CsPbBr₃ Solar Cells: Controlled
31 Film Growth through Layer-by-Layer Quantum Dot Deposition. *Chem. of Mater.*
32 **2017**, *29*, 9767–9774.
33
34 (28) Creutz, S. E.; Crites, E. N.; De Siena, M. C.; Gamelin, D. R. Anion Exchange in
35 Cesium Lead Halide Perovskite Nanocrystals and Thin Films Using Trimethylsilyl
36 Halide Reagents. *Chem. Mater.* **2018**, *30*, 4887–4891.
37
38 (29) Hazarika, A.; Zhao, Q.; Gauding, E. A.; Christians, J. A.; Dou, B.; Marshall, A. R.;
39 Moot, T.; Berry, J. J.; Johnson, J. C.; Luther, J. M. Perovskite Quantum Dot
40 Photovoltaic Materials beyond the Reach of Thin Films: Full-Range Tuning of A-
41 Site Cation Composition. *ACS Nano* **2018**, *12*, 10327-10337.
42
43
44
45
46
47
48
49
50
51
52
53
54
55
56
57
58
59
60

Pursuant to the DOE Public Access Plan, this document represents the authors' peer-reviewed, accepted manuscript.
The published version of the article is available from the relevant publisher.

- 1
2
3
4 (30) Cariou, R.; Benick, J.; Beutel, P.; Razek, N.; Flötgen, C.; Hermle, M.; Lackner, D.;
5 Glunz, S. W.; Bett, A. W.; Wimplinger, M.; et al. Monolithic Two-Terminal III–V//Si
6 Triple-Junction Solar Cells With 30.2% Efficiency Under 1-Sun AM1.5g. *IEEE J.*
7 *Photov.* **2017**, *7*, 367–373.
8
9
10 (31) Shockley, W.; Queisser, H. J. Detailed Balance Limit of Efficiency of *p-n* Junction
11 Solar Cells. *J. Appl. Phys.* **1961**, *32*, 510–519.
12
13 (32) Ghosh, D.; Ali, M. Y.; Chaudhary, D. K.; Bhattacharyya, S. Dependence of Halide
14 Composition on the Stability of Highly Efficient All-Inorganic Cesium Lead Halide
15 Perovskite Quantum Dot Solar Cells. *Sol. Energ. Mat. Sol. C.* **2018**, *185*, 28–35.
16
17 (33) Akkerman, Q. A.; Gandini, M.; Di Stasio, F.; Rastogi, P.; Palazon, F.; Bertoni, G.;
18 Ball, J. M.; Prato, M.; Petrozza, A.; Manna, L. Strongly Emissive Perovskite
19 Nanocrystal Inks for High-Voltage Solar Cells. *Nat. Energy* **2016**, *2*, 16194.
20
21 (34) Sanehira, E. M.; Marshall, A. R.; Christians, J. A.; Harvey, S. P.; Ciesielski, P. N.;
22 Wheeler, L. M.; Schulz, P.; Lin, L. Y.; Beard, M. C.; Luther, J. M. Enhanced Mobility
23 CsPbI₃ Quantum Dot Arrays for Record-Efficiency, High-Voltage Photovoltaic Cells.
24 *Sci. Adv.* **2017**, *3*, eaao4204.
25
26 (35) Wheeler, L. M.; Sanehira, E. M.; Marshall, A. R.; Schulz, P.; Suri, M.; Anderson, N.
27 C.; Christians, J. A.; Nordlund, D.; Sokaras, D.; Kroll, T.; et al. Targeted Ligand-
28 Exchange Chemistry on Cesium Lead Halide Perovskite Quantum Dots for High-
29 Efficiency Photovoltaics. *J. Am. Chem. Soc.* **2018**, *140*, 10504–10513.
30
31 (36) Yuan, J.; Ling, X.; Yang, D.; Li, F.; Zhou, S.; Shi, J.; Qian, Y.; Hu, J.; Sun, Y.; Yang,
32 Y.; et al. Band-Aligned Polymeric Hole Transport Materials for Extremely Low
33 Energy Loss α -CsPbI₃ Perovskite Nanocrystal Solar Cells. *Joule* **2018**, *2*, 2450-
34 2463
35
36 (37) Xue, J.; Lee, J.-W.; Dai, Z.; Wang, R.; Nuryyeva, S.; Liao, M. E.; Chang, S.-Y.;
37 Meng, L.; Meng, D.; Sun, P.; et al. Surface Ligand Management for Stable FAPbI₃
38 Perovskite Quantum Dot Solar Cells. *Joule* **2018**, *2*, 1866–1878.
39
40 (38) Denton, A. R.; Ashcroft, N. W. Vegard's Law. *Phys. Rev. A* **1991**, *43*, 3161–3164.
41
42 (39) Protesescu, L.; Yakunin, S.; Kumar, S.; Bär, J.; Bertolotti, F.; Masciocchi, N.;
43 Guagliardi, A.; Grotevent, M.; Shorubalko, I.; Bodnarchuk, M. I.; et al. Dismantling
44
45
46
47
48
49
50
51
52
53
54
55
56
57
58
59
60

Pursuant to the DOE Public Access Plan, this document represents the authors' peer-reviewed, accepted manuscript.
The published version of the article is available from the relevant publisher.

- 1
2
3
4 the “Red Wall” of Colloidal Perovskites: Highly Luminescent Formamidinium and
5 Formamidinium–Cesium Lead Iodide Nanocrystals. *ACS Nano* **2017**, *11*, 3119–
6 3134.
7
8
9 (40) Wang, P; Zhang, X; Zhou, Y; Jiang, Q; Ye, Q; Chu, Z; Li, X; Yang, X; Yin, Z; You,
10 J. Solvent-controlled growth of inorganic perovskite films in dry environment for
11 efficient and stable solar cells. *Nat. Comm.* **2018**, *9*, 2225
12
13
14 (41) Savenije, T. J.; Ferguson, A. J.; Kopidakis, N. & Rumbles, G. Revealing the
15 Dynamics of Charge Carriers in Polymer:Fullerene Blends Using Photoinduced
16 Time-Resolved Microwave Conductivity. *J. Phys. Chem. C* **2013**, *117*, 24085–
17 24103
18
19
20
21 (42) Reid, O. G. et al. Quantitative analysis of time-resolved microwave conductivity
22 data. *J Phys D Appl Phys* **2017**, *50*, 493002
23
24
25
26
27
28
29
30
31
32
33
34
35
36
37
38
39
40
41
42
43
44
45
46
47
48
49
50
51
52
53
54
55
56
57
58
59
60